Improving Ride Comfort of a Soil Compactor based on the NSS Embedded into the Seat's Semiactive Suspension

Jinyu Jiang

chool of Mechanical and Electrical Engineering, Hubei Polytechnic University, China.
Hubei Key Laboratory of Intelligent Conveying Technology and Device, Hubei Polytechnic University, China.

Lujian Min, Yang Jing, Shiding Ding and Machun Yu

College of Mathematics and Physical Science, Handan University, China.

Wangxiang Jie

College of Mechanical Engineering, Suzhou University, China.

(Received 26 November 2022; accepted 13 January 2023)

Three dynamic models (1-D, 2-D, and 3-D) of a soil compactor are established to research the vehicle's ride comfort via numerical simulation and experiment. Based on the efficiency of the semi-active control (SAC) of the Fuzzy-PID controller and the negative stiffness structure (NSS), a new suspension of the driver's seat equipped with the SAC and NSS is proposed to further improve the soil compactor's ride comfort under the various working conditions of the vehicle on the elastoplastic soil ground. The reduction of the root-mean-square seat acceleration (a_{ws}) in the time domain and the power-spectral-density seat acceleration (PSD) in the frequency domain is chosen as the objective function. The study indicates that the seat's acceleration response in the time domain with the 1-D, 2-D, and 3-D models of the soil compactor is similar. However, the a_{ws} and maximum PSD acceleration of the driver's seat with the 1-D model are higher than that of the 3-D model by 35.9% and 58.5%, while the acceleration response and PSD acceleration of the driver's seat with the simulation of the 3-D model are similar to the experiment. Therefore, the different dynamic models of the vehicle remarkably affect the investigation result. With the driver's seat suspension equipped with the SAC and NSS, the a_{ws} and maximum PSD acceleration of the driver's seat are strongly decreased by 80.1% and 87.6% compared to the seat's passive suspension without the SAC and NSS. Additionally, these values are also lower than that of oth the SAC and NSS under various simulation conditions. Consequently, the driver's seat suspension equipped with the SAC and NSS could be used to further improve the ride comfort of the soil compactor.

1. INTRODUCTION

Existing studies indicated that the driver seat's vertical acceleration and the cab's pitching angle of soil compactors were very high, and they greatly affected the ride comfort and working efficiency of the driver.[1–3] To improve the vehicle's ride comfort, the traditional rubber isolations of the soil compactor cab had been replaced by using hydraulic mounts.[4] The semi-active control of the cab's hydraulic mounts was studied based on a combination between the fuzzy controller and proportional-integral-derivative controller (Fuzzy-PID controller).[5,6] The soil compactor's ride comfort had been significantly improved. However, the vertical vibration response of the driver's seat was still very high according to the standard of ISO 2631-1 (1997).[7] Especially in the condition of the soil compactor moving and compacting on the elastoplastic soil ground. This is a problem that still exists and it has not been completely resolved yet. To solve this issue, the passive suspension of the soil compactor seat needs to be studied and improved.

In the research of the seat's suspension systems, in order to improve the driver's ride comfort, the air spring system of the driver's seat had been used.[8,9] Additionally, based on the optimal control of the fuzzy controller, the genetic algorithm, and the Fuzzy-PID controller, the semi-active control (SAC) of the driver's seat suspension was also studied and developed.[10–12] The results showed that the SAC of the driver's seat suspension using the Fuzzy-PID controller remarkably improved the vertical acceleration response of the driver's seat. In addition, a new design of the negative stiffness structure (NSS) using steel springs had been also researched and applied for the seat passive suspension of the vehicles.[13–15] The different structures of the NSS using the steel spring, air spring, and roller spring were studied to improve the NSS's efficiency.[16] The optimization of the NSS's design parameters was also given to enhance the isolation efficiency of the NSS.[17,18] The result showed that the seat passive suspension added by the NSS greatly improved the driver's seat in both the time and frequency regions. Experimental studies were also performed to prove the actual efficiency of the NSS.[15,19] Besides, based on the magnetic char-

acteristic, the magnetic negative stiffness dampers were researched and applied to the seat suspension.[20,21] The vibration response of the seat was also significantly reduced. However, the seat's acceleration in the low-frequency region was still high. Thus, the electromagnetic negative stiffness was also applied to the low-frequency nonlinear vibration isolation to reduce the acceleration response in the low-frequency domain of the isolation system.[22–24] The results showed that the vibration response of the seat in the low-frequency domain was remarkably decreased. However, based on the existing studies of the seat suspension using the SAC and seat suspension embedded by the NSS, there are still some issues that need to be solved as follows:

- The seat suspension using the SAC and the seat suspension equipped with the NSS had been studied independently of each other, and their isolation efficiency had been demonstrated. However, if the seat suspension is combined by both SAC and NSS, is its isolation efficiency better than the SAC or the NSS? This issue has not been evaluated in existing studies yet.

- In the study of the vibration characteristic and efficiency of the SAC or NSS of the seat suspension, most of the 1-D dynamic model of the vehicle and seat was used. The isolation efficiency of the seat suspension using the SAC or NSS obtained was very high.[9–15,20–24] However, the seat suspension using the SAC or NSS is installed on the 3-D vehicle structure. The use of the 1-D model of the vehicle and seat to evaluate the efficiency of the seat suspension using the SAC or NSS may not fully reflect their actual efficiency. Thus, the efficiency of the SAC or NSS of the seat suspension should be accurately evaluated based on the 3-D dynamic model of the vehicle and seat. However, this issue has not yet been considered.

- In the study models of the seat suspension using the SAC and NSS, the vibration excitation was viewed as the random excitation of the rigid road surface to evaluate their efficiency. However, in some vehicles, especially soil compactors, the vehicle mainly moves and works on the elastoplastic soil ground with a deformable terrain surface. Accordingly, the vibration excitation of an off-road terrain surface can also affect the efficiency and stability of the seat suspension using the SAC or NSS. This issue also needs to be studied and evaluated.

Therefore, to improve the soil compactor's ride comfort and clarify some of the above existing problems, three different types of the soil compactor's seat suspension including: (1) the seat suspension controlled by the SAC of the Fuzzy-PID controller, (2) the seat suspension embedded by the NSS, and (3) the seat suspension equipped with both SAC and NSS are proposed and studied. Three different dynamic models of the soil compactor including the 1-D model, 2-D model, and 3-D model are established to evaluate the efficiency and stability of three seat suspension models under the conditions of the soil compactor moving and compacting on the elastoplastic soil ground. The experimental study of the soil compactor is then given to validate the mathematical model and numerical simulation method. The reduction of the root-mean-square acceleration of the driver's seat in the time domain and power-spectral-density acceleration (PSD) of the driver's seat in the frequency domain is chosen as the objective function.

2. MATHEMATICAL MODELS

2.1. Soil Compactor's Different Dynamic Models

The soil compactor's structure includes the driver's seat, cab, vehicle floor, wheel, and drum. The driver's seat is connected to the cab floor via the seat suspension. The cab's floor is connected to the rear vehicle floor via the cab isolations. The front floor and rear floor of the vehicle are connected by a swivel joint. The front vehicle floor is connected with the drum via rubber mounts. To evaluate the ride comfort of the soil compactor and the efficiency of the seat suspension equipped with the SAC and NSS, three different dynamic models including the 1-D model, 2-D model, and 3-D model of the soil compactor are established, as modeled in Fig. 1a, 1b, and 1c, respectively. Where m_s, m_c, m_{fb}, m_{rb}, and m_d is the mass of the driver's seat, cab, front/rear vehicle floor, and drum; z_s, z_c, z_{fb}, z_{rb}, and z_d is the displacement of the driver's seat, cab, front/rear vehicle floor, and drum; ϕ_c and ϕ_{rb} are the pitching angles of the cab and rear vehicle floor; θ_c, θ_{fb}, θ_{rb}, and θ_d are the rolling angles of the cab, front/rear vehicle floor, and drum; k_s, k_c, k_d, k_w and c_s, c_c, c_d, c_w are the stiffness and damping coefficients of the isolation systems of the driver's seat, cab, front vehicle floor, and wheel; c_h is the damping coefficient of the fluid in the hydraulic mount; u is the control force of the Fuzzy-PID controller; k_n is the horizontal stiffness of the NSS; l_{1-8} and b_{1-5} are the distances of the vehicle in the x- and y-directions; v_0 and q_w are the vehicle's moving speed and the excitation of the road surface, respectively.

To simplify the calculation of the vehicle's vibration equations, the following assumptions are made: (1) The front/rear vehicle floor and cab floor are absolutely hard and their elastic deformation is very small and is also ignored; (2) The excitation of the vehicle is mainly generated by the soil ground and vibratory drum in the z-direction; (3) The displacement of the front/rear vehicle floor, cab, and driver's seat around their equilibrium position is very small and is ignored; and (4) The gap of the articulation connection between the front floor and rear floor of the soil compactor in 2-D and 3-D models is very small and it insignificantly affects the vehicle's pitching angle. Based on the different dynamic models in Fig. 1, the vehicle's vibration equations are written as:

(1) The 1-D dynamic model of the vehicle:

$$\begin{aligned} m_s\ddot{z}_s &= -F_s; \\ m_c\ddot{z}_c &= F_s - F_c; \\ m_b\ddot{z}_b &= F_c - F_d. \end{aligned} \tag{1}$$

(2) The 2-D dynamic model of the vehicle:

$$m_s\ddot{z}_s = -F_s;$$

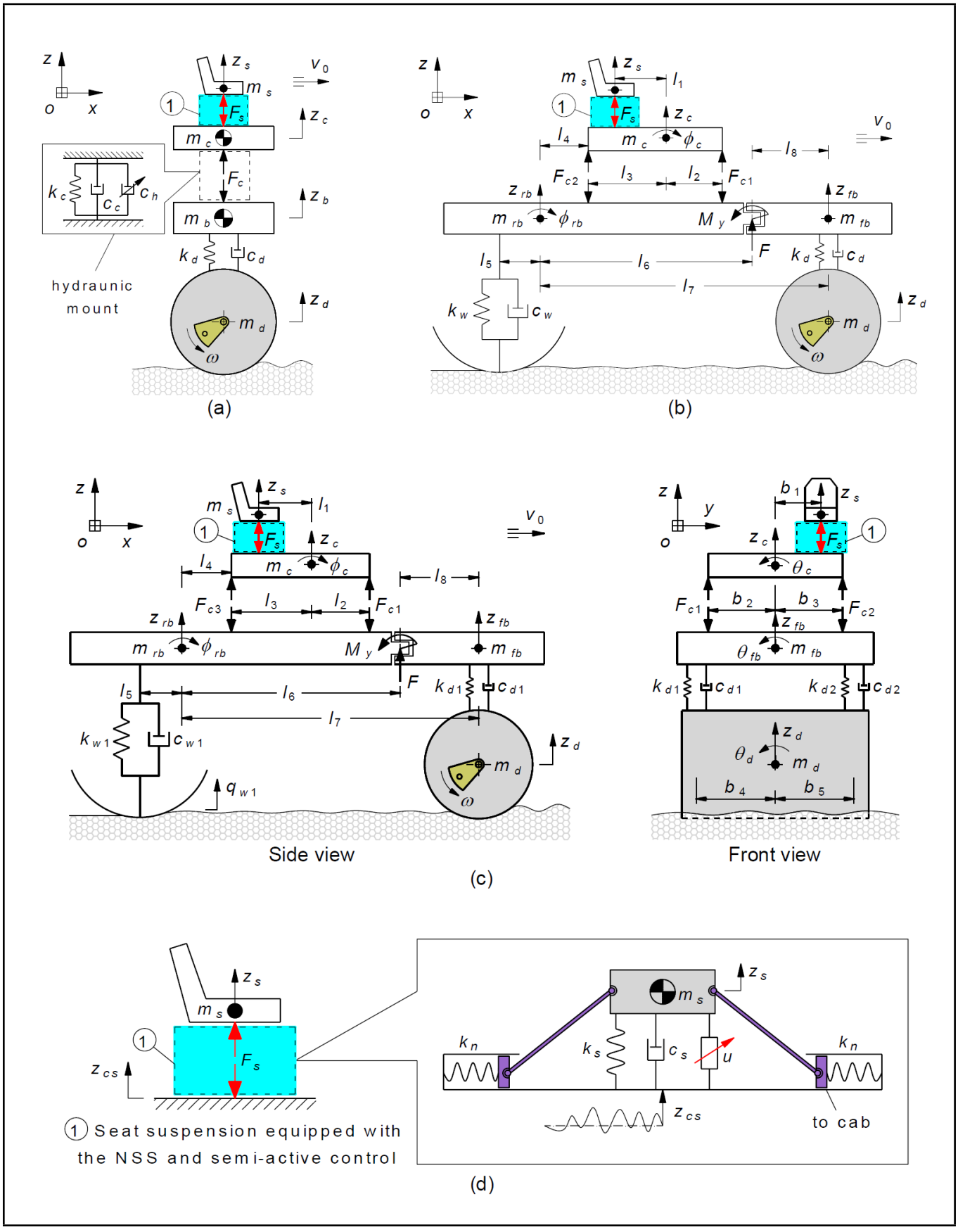

Figure 1. The 1-D dynamic model (a), 2-D dynamic model (b), 3-D dynamic model of the soil compactor (c), and model of seat suspension equipped with the SAC and NSS (d).

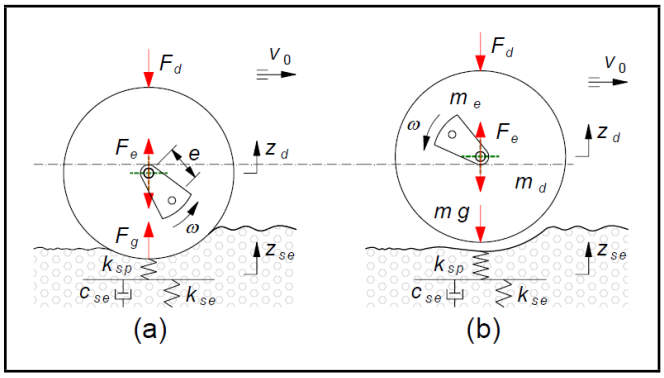

Figure 2. The interaction model of the drum and elastoplastic soil ground with loading phase (a) and drum-hop phase (b).

$$\begin{aligned} m_c\ddot{z}_c &= F_s - F_{c1} - F_{c2};\\ I_{cy}\ddot{\phi}_c &= l_1F_s + l_2F_{c1} - l_3F_{c2};\\ m_{fb}\ddot{z}_{fb} &= F - F_d;\\ m_{rb}\ddot{z}_{rb} &= F_{c1} + F_{c2} - F_w - F;\\ I_{rby}\ddot{\phi}_{rb} &= l_6F + M_y - l_5F_w - lF_{c1} - l_4F_{c2}. \end{aligned} \tag{2}$$

(3) The 3-D dynamic model of the vehicle:

$$\begin{aligned} m_s\ddot{z}_s &= -F_s;\\ m_c\ddot{z}_c &= F_s - \sum_{i=1}^{4} F_{ci};\\ I_{cy}\ddot{\phi}_c &= l_1F_s + \sum_{i=1}^{2} l_2F_{ci} - \sum_{i=3}^{4} l_3F_{ci};\\ I_{cx}\ddot{\theta}_c &= b_1F_s + \sum_{i=1}^{4}(-1)^{i+1}b_nF_{ci};\\ m_{fb}\ddot{z}_{fb} &= F - \sum_{j=1}^{2} F_{dj};\\ I_{fbx}\ddot{\theta}_{fb} &= \sum_{j=1}^{2}(-1)^{j+1}b_{j+3}F_{dj};\\ m_{rb}\ddot{z}_{rb} &= \sum_{i=1}^{4} F_{ci} - \sum_{j=1}^{2} F_{wj} - F;\\ I_{rby}\ddot{\phi}_{rb} &= l_6F + M_y - \sum_{j=1}^{2} l_5F_{wj} + \sum_{i=1}^{4} \alpha lF_{ci};\\ I_{rbx}\ddot{\theta}_{rb} &= \sum_{i=1}^{4}(-1)^{i}b_nF_{ci} + \sum_{j=1}^{2}(-1)^{j+1}b_{j+3}F_{wj}; \end{aligned} \tag{3}$$

where: if $i = 1, 2$ then $\alpha = -1$, $l = l_2 + l_3 + l_4$, and $n = i + 1$; if $i = 3, 4$ then $\alpha = +1$, $l = l_4$, and $n = i - 1$; $F = F_{d1} + F_{d2}$; $M_x = b_4F_{d1} + b_5F_{d2}$; $M_y = l_8F$; F_s is the force response of the driver's seat suspension; F_c is the force response of the cab's isolation system; F_d is force response of the vibratory drum's isolation; and F_w is the force response of the wheel in the 2-D and 3-D models, respectively.

In Eqs. (1), (2), and (3), the F_s is determined in Section 3. The F_c, F_d, and F_w are determined in the following subsections.

2.2. The F_c of the Cab Isolations

Based on the existing studies on the soil compactor,[2–4] the efficiency of the cab's hydraulic mounts in improving the soil compactor's ride comfort was better than that of the rubber and pneumatic mounts. Thus, the cab isolations in Fig. 1a, 1b, and 1c have been also used by the hydraulic mounts to improve the vehicle's ride comfort. The F_c in each model of the soil compactor is expressed by:[4,5]

- With the 1-D dynamic model of the vehicle:

$$\begin{aligned} F_c &= k_cz_{cb} + c_c\dot{z}_{cb} + c_h\dot{z}_{cb}|\dot{z}_{cb}|;\\ z_{cb} &= z_c - z_b. \end{aligned} \tag{4}$$

- With the 2-D model dynamic model of the vehicle:

$$\begin{aligned} F_{ci} &= k_{ci}z_{cbi} + c_{ci}\dot{z}_{cbi} + c_{hi}\dot{z}_{cbi}|\dot{z}_{cbi}|;\\ z_{cbi} &= z_c - z_{rb} + (-1)^i l_{i+1}\phi_c - l\phi_{rb}; \end{aligned} \tag{5}$$

where if $i = 1$ then $l = l_2 + l_3 + l_4$ and if $i = 2$ then $l = l_4$.

- With the 3-D model dynamic model of the vehicle:

$$\begin{aligned} F_{ci} &= k_{ci}z_{cbi} + c_{ci}\dot{z}_{cbi} + c_{hi}\dot{z}_{cbi}|\dot{z}_{cbi}|;\\ z_{cbi} &= z_c - z_{rb} + (-1)^{\alpha+1}l_{\alpha+1}\phi_c - l\phi_{rb} +\\ &\quad (-1)^{i+1}b_\delta(\theta_c - \theta_{rb}); \end{aligned} \tag{6}$$

where if $i = 1, 2$ then $\alpha = 1$, $l = l_2 + l_3 + l_4$, and $\delta = i + 1$; if $i = 3, 4$ then $\alpha = 2$, $l = l_4$, and $\delta = i - 1$.

2.3. The F_d of the Vibratory Drum's Isolation

The soil compactor mainly moved and worked on the elastoplastic soil ground to compress the soil ground.[1–4] Therefore, the vibration excitation of the drum is generated by both the excitation force $F_e = m_e e\omega^2 \sin\omega t$ of the rotating eccentric mass m_e and the interaction between the drum and elastoplastic soil ground. To determine the F_d, a dynamic model of the drum and elastoplastic soil ground interaction is established, as plotted in Fig. 2, where $m = m_d + m_{fb}$; e and ω are the eccentricity and rotational velocity of m_e; k_{se} and k_{sp} are the elastic and plastic stiffness parameters of the elastoplastic soil ground; z_{es} and c_{es} are the deformation and elastic damping coefficient of the elastoplastic soil ground; and F_g is the restoring force of the elastoplastic soil ground generated by the elastic soil layer in the compacting process of the drum.

The vibration equation of the drum and elastoplastic soil ground interaction is determined by:[1,2,4]

$$\begin{aligned} m_d\ddot{z}_d &= F_d - F_g + F_e;\\ F_g &= k_{ps}[z_d - (q - z_{es})] = c_{es}\dot{z}_{es} + k_{es}z_{es};\\ F_d &= \begin{cases} k_d(z_b - z_d) + c_d(\dot{z}_b - \dot{z}_d) & \text{1-D model;}\\ k_d(z_{fb} - z_d) + c_d(\dot{z}_{fb} - \dot{z}_d) & \text{2-D model;}\\ k_{dj}(z_{fbj} - z_{dj}) + c_{dj}(\dot{z}_{fbj} - \dot{z}_{dj}) & \text{3-D model;} \end{cases} \end{aligned} \tag{7}$$

where $z_{fbj} - z_{dj} = z_{fb} - z_d + (-1)^j b_{3+j}(\theta_{fb} - \theta_d)$, $j = 1, 2$.

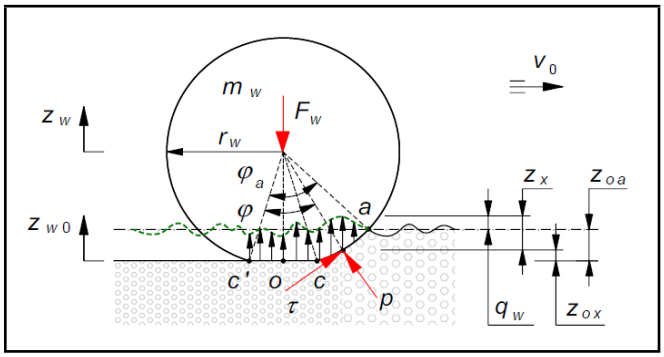

Figure 3. The interaction model between the wheel and terrain.

In each cycle interaction of the drum on the elastoplastic soil ground, there are two or three distinct phases including the loading, unloading, and drum-hop phases.[1,2] At the loading phase, the compressive force of the drum compacts on the soil ground due to the drum moving downward and it is the elastoplastic deformation phase. During the unloading phase, the contact of the drum and soil ground is retained whereas the drum moves upward. The elastic deformation of the soil ground is recovered while the plastic deformation represents the soil compaction. At the drum-hop phase, the contact between the drum and soil ground is broken, and the elastic characteristic of the soil ground is recovered whereas the plastic characteristic of the soil ground vanishes. Based on the study result published by Adam and Kopf,[1] the change of elastoplastic properties under the interaction of the drum and elastoplastic soil ground is described by:

$$\varepsilon\gamma m_d \dddot{z}_d + m_d \ddot{z}_d = \varepsilon\gamma \dot{F}_d + F_d + \delta mg - \varepsilon c_{es}\dot{z}_d + (\varepsilon - 1)k_{ps}z_d + \varepsilon\gamma\dot{F}_e + F_e; \quad (8)$$

where if

$$\begin{cases} P > 0, \dot{z}_d > 0 & \text{then } \delta = 0, \gamma > 0, 1 > \varepsilon > 0, \text{ (Loading);} \\ P > 0, \dot{z}_d < 0 & \text{then } \delta = \gamma = 0, \varepsilon = 1, \text{ (Unloading);} \\ P = 0 & \text{then } \delta = 1, \gamma = \varepsilon = 0, \text{ (Drum-hop);} \end{cases}$$

$P = F_g + mg$; $\varepsilon = k_{ps}/(k_{ps} + k_{es})$; and $\gamma = c_{es}/k_{ps}$.

By combining Eqs. (7) and (8), the F_d is then calculated.

2.4. The F_w of the Wheel and Terrain Interaction

When the soil compactor is moving on the elastoplastic soil ground, under the impaction of the static-dynamic load of the wheel on the soil ground, the contact region between the wheel and soil ground may appear two deformable regions including (1) the deformable region of both the soil ground and wheel (*c'oc* region) and (2) the only deformation of the soil ground (*ca* region), as plotted in Fig. 3. Where z_x, z_{w0}, and z_w are the sinkage of the soil ground, static deformation of the wheel, and displacement of the wheel axle; r_w and m_w are the radius and mass of the wheel, respectively.

The vertical reaction force generated by the press p and stress τ of the soil ground in two deformable regions of *c'oc* and *ca* are determined by:[25,26]

$$F_{gw} = \int_0^{\varphi_a} B_w r_w (p\cos\varphi + \tau\sin\varphi)d\varphi; \quad (9)$$

Table 1. Lumped parameter of the off-road terrain surface.

Levels	Good	Medium	Poor	Very poor
n_0	2.25	2.25	2.14	2.14
$G(\varpi_0) \times 10^{-6}$ / m^3 cyc^{-1}	199.8	973.9	3782.5	102416

where $p = (k/B_w + k_\theta)z_x^n$; $\tau = (c + p\tan\theta)(1 - e^{-j/K})$; $z_x = q_w + z_{oa} - z_{ox} = q_w + z_w - z_{w0} - z_{ox}$; B_w is the width of the wheel; k_φ is the stiffness of the terrain's internal friction; k_c is the stiffness of the terrain's sinkage; and n is the sinkage exponent ($n = 1.01$), respectively.

Therefore, the F_w of the wheel in the 2-D and 3-D models are expressed by:

- With the 2-D dynamic model of the vehicle:

$$F_w + F_{gw} - m_w g = 0;$$
$$F_w = k_w(\dot{z}_{rb} - l_5\dot{\phi}_{rb} - z_w) + c_w(\dot{z}_{rb} - l_5\dot{\phi}_{rb} - \dot{z}_w). \quad (10)$$

- With the 3-D dynamic model of the vehicle:

$$F_{wj} + F_{gwj} - m_{wj}g = 0, \quad (j = 1, 2);$$
$$F_{wj} = k_{wj}(z_{rb} - l_5\phi_{rb} + (-1)^j b_{j+3}\theta_{rb} - z_{wj}) + c_{wj}(\dot{z}_{rb} - l_5\dot{\phi}_{rb} + (-1)^j b_{j+3}\dot{\theta}_{rb} - \dot{z}_{wj}). \quad (11)$$

To calculate the F_d and F_w in Eq. (7) and Eqs. (10)–(11), the random excitation q_w of the soil ground surface needs to be determined. Based on the PSD of the random surface of the deformable soil ground $G(\varpi)$ and ISO/TC108/SC2/WG4,[27,28] the $G(\varpi)$ was calculated by:

$$G(\varpi) = G(\varpi_0)\left(\frac{\varpi}{\varpi_0}\right)^{-n_0}, \quad \begin{cases} n_0 = 3, & \varpi \le \varpi_0; \\ n_0 = 2.25, & \varpi > \varpi_0; \end{cases} \quad (12)$$

where $\varpi_0 = 1/2\pi$ cycle m^{-1} is reference spatial frequency; $G(\varpi_0)$ is the reference density of the random road surface.

Based on the PSD value of $G(\varpi)$ in Eq. (12) at a forward speed v_0 of the soil compactor and the white noise signal W of the random function, the q is thus expressed by:[11]

$$\dot{q}_w + 2\pi\varpi_0 v_0^2 q_w = 2\pi\varpi_0\sqrt{G(\varpi)v_0}W. \quad (13)$$

Mitschke proposed the PSD of the deformable soil ground's random surface via four levels including the good surface, medium surface, poor surface, and very poor surface,[29] as listed in Table 1. Thus, the q_w could be built by choosing one of the good, medium, poor, or very poor surfaces.

Based on the parameters of a poor level of the soil ground surface in Table 1 when the soil compactor is moving at $v_0 = 3$ km h^{-1}, the PSD value and profile of q_w in the frequency and time regions are plotted in Fig. 4a and 4b, respectively. This excitation is then used to simulate the soil compactor dynamic models in Fig. 1.

3. MODEL OF SEAT SUSPENSION

3.1. Seat Suspension Equipped with SAC and NSS

In the passive suspension of the soil compactor seat, the steel spring and damper with the passive stiffness (k_s) and pas-

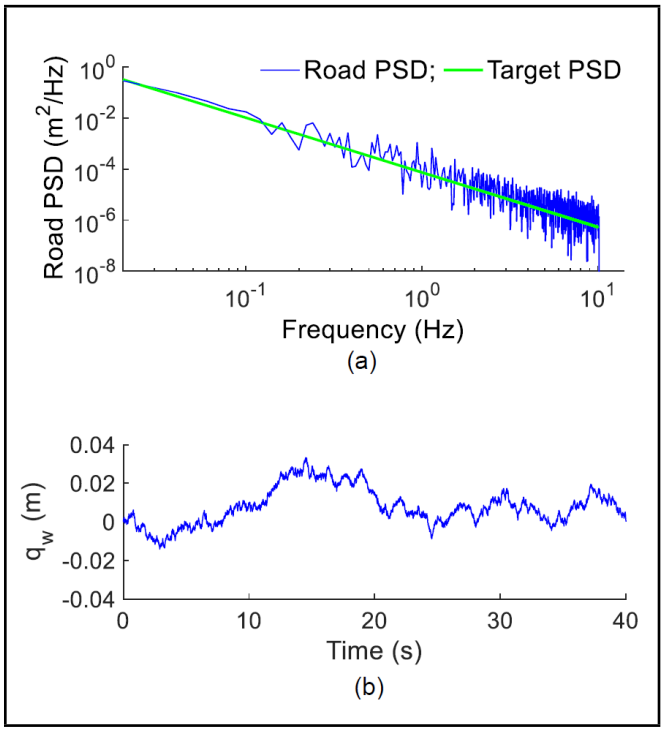

Figure 4. The PSD value (a) and profile surface of the poor terrain surface (b).

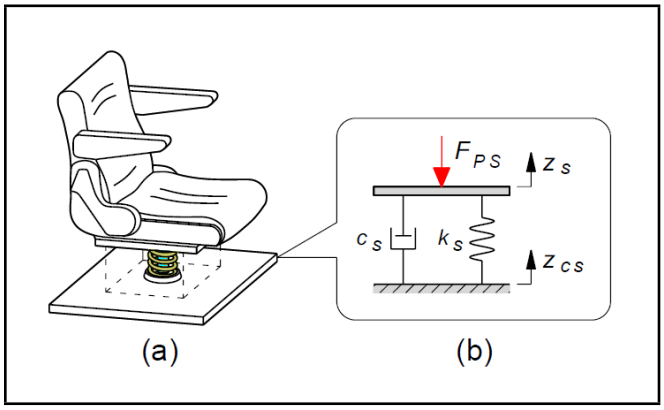

Figure 5. The passive suspension structure of the seat (a) and its lumped parameter model (b).

sive damping (c_s) coefficients had been mainly applied.[2–4] Its structure and dynamic model are plotted in Fig. 5a and 5b.

Based on the soil compactor dynamic model in Fig. 1 and the lumped parameter model of the seat passive suspension in Fig. 5b, its force response is written by:

$$m_s\ddot{z}_s = F_s = F_{PS} = k_s(z_s - z_{cs}) + c_s(\dot{z}_s - \dot{z}_{cs});$$
$$z_{cs} = \begin{cases} z_c & \text{with 1-D;} \\ z_c - l_1\phi_c & \text{with 2-D;} \\ z_c - l_1\phi_c - b_1\theta_c & \text{with 3-D.} \end{cases} \quad (14)$$

The ride comfort of the soil compactors was mainly researched based on the improvement of the cab isolation systems while the seat's isolation was used by the passive suspension,[4–6] thus, the driver's ride comfort is very difficult to ensure according to the ISO 2631-1.[7] To solve this issue, apart from using the cab's hydraulic mounts, the passive suspension of the seat has been researched and replaced by the seat suspension equipped with the SAC and NSS. Its structure and dynamic

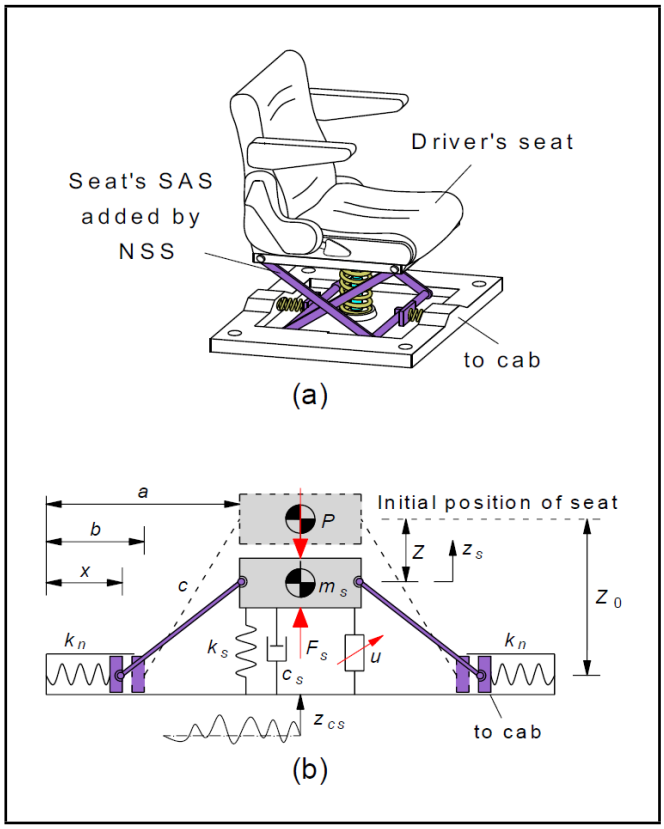

Figure 6. The structure of the seat suspension equipped with the SAC and NSS (a) and (b) its lumped parameter model.[15,19]

model are plotted in Fig. 6a and 6b. Where k_n is the stiffness coefficient of two steel springs of the NSS installed horizontally and symmetrically on the cab floor; a is the distance between the wall and seat; b is the initial length of the horizontal spring; c is the length of the hard guide bar used to link between the driver's seat and horizontal spring; x is the length after deformation of the horizontal spring; and Z_0 is the distance between the seat's initial position and cab's floor.[15,18,19]

To reduce complexity in the calculation of the seat suspension equipped with the SAC and NSS, the following assumptions are made: (1) The excitation of the seat suspension from the cab floor is only in the vertical direction; (2) The mass of the hard guide bar of the NSS is very small and it is ignored; and (3) The sliding friction at the joints between the hard guide bar and seat, and between the hard guide bar and horizontal spring is very small and also ignored.

Therefore, under the impaction of the static load of the driver's seat ($P = m_s \times g$), the driver's seat suspension is deformed downward by Z. The force response F_s is thus expressed as follows:

$$F_s = F_R + F_D;$$
$$F_R = k_s Z + 2k_n(b - x)\frac{Z_0 - Z}{a - x};$$
$$F_D = c_s\dot{Z} + u; \quad (15)$$

where F_D is the passive and active damping force of the damper and F_R is the total restoring force of the vertical and horizontal springs.

Based on the seat's equilibrium position and NSS's geomet-

rical dimension, the x and Z_0 are determined by:[19]

$$x = a - \sqrt{c^2 - (Z_0 - Z)^2} \text{ and } Z_0 = \sqrt{c^2 - (a-b)^2}. \quad (16)$$

By substituting Eq. (16) into (15), F_s is rewritten by:

$$\begin{aligned} F_s &= k_s Z + 2k_n \left(\frac{b-a}{\sqrt{c^2 - (Z_0 - Z)^2}} + 1 \right) (Z_0 - Z) + F_D \\ &= k_s Z + 2\alpha k_s \left(\frac{1-\beta_2}{\sqrt{\beta_1^2 - \frac{(Z_0 - Z)^2}{b^2}}} + 1 \right) (Z_0 - Z) + F_D; \end{aligned} \quad (17)$$

where $\alpha = k_n/k_s$, $\beta_1 = c/b$, and $\beta_2 = a/b$ are the ratios of the stiffness and geometrical dimension of the NSS.

Under the excitation of z_{cs} from the cab floor at the position of the seat suspension, as shown in Fig. 6b, the vibration of the seat at the static equilibrium position is then generated by z_s. Therefore, the motion equation of the seat in Eqs. (1), (2), and (3) is rewritten by:

$$\begin{aligned} m_s \ddot{z}_s = -\Big(& k_s(z_s - z_{cs}) + 2\alpha k_s(\Phi + 1)(Z_0 - Z) + \\ & c_s(\dot{z}_s - \dot{z}_{cs}) + u \Big); \end{aligned} \quad (18)$$

where $\Phi = (1-\beta_2)/\sqrt{\beta_1^2 - (Z_0 - Z)^2/b^2}$, $z_s - z_{cs} = Z_0 - Z$, and z_{cs} has been determined in Eq. (14).

Equation (18) is then applied to compute the isolation efficiency of the seat suspension equipped with the SAC and NSS.

3.2. The Control of the Seat Suspension with the Fuzzy-Pid Controller

The PID controller has a simple structure and strong efficiency. It is mainly used in industrial process control. However, the control efficiency of the PID controller greatly depends on the selection of the parameters of k_p, k_i, and k_d. The technique of Ziegler-Nichols is then applied to optimize the parameters of k_p, k_i, and k_d. However, the maximum efficiency of the PID with its optimal parameters is only obtained when the system works in a specified condition. Conversely, the fuzzy controller can control the system under all of the different operating conditions. However, the efficiency and stability of the fuzzy controller are quite low.[5,11] To overcome the disadvantages of the fuzzy controller and PID controller, a controller that is combined with the fuzzy controller and PID controller (Fuzzy-PID controller) is proposed to control the active damping force u for the seat suspension of the soil compactor. The control model is shown in Fig. 7.

The fuzzy controller is designed by two input variables of the displacement "$e = z_s - z_{cs}$" and velocity "$ec = \dot{e}$" of the seat suspension and three output variables of the proportionality factors K_p, K_i, and K_d, respectively. Concurrently, the PID controller is designed by three input variables of the proportional k_p, integral k_i, and derivative k_d (these parameters are changed and depend on three output parameters K_p, K_i, and K_d); and one output value of the active damping force "u".

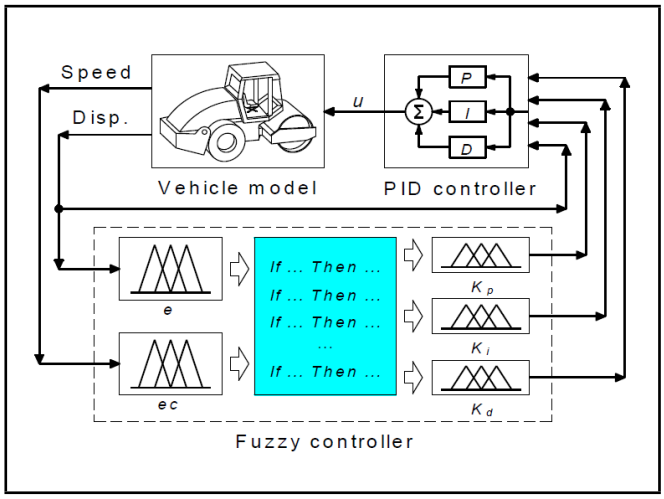

Figure 7. The control model of the Fuzzy-PID controller for the vibratory roller's seat isolation.

The active damping force "u" is given by:

$$u = k_p e + k_i \int_0^t e\, dt + k_d \dot{e}. \quad (19)$$

Based on the method of Ziegler Nichols and the control model of the soil compactor seat, the initial parameters of k_p, k_i, and k_d in Eq. (19) are obtained by $k_p = 2305$, $k_i = 30$, and $k_d = 2.0$. To determine the optimal parameters k_ν (subscript ν denotes p, i, and d of k_p, k_i, and k_d), the value of k_ν is assumed to change from $k_\nu^{\min}$ to $k_\nu^{\max}$. Based on the initial proportionality factors of the PID controller, the range of each value k_ν is then chosen by $1000 \le k_p \le 3500$, $1.0 \le k_i \le 200$, and $0.1 \le k_d \le 20$. Thus, the K_ν of the fuzzy controller is calculated via the variables k_ν of the PID controller as follows:[25]

$$\begin{aligned} K_\nu &= \frac{k_\nu - k_\nu^{\min}}{k_\nu^{\max} - k_\nu^{\min}}, \ (0 \le K_\nu \le 1); \\ \Rightarrow k_\nu &= k_\nu^{\min} + (k_\nu^{\max} - k_\nu^{\min}) K_\nu. \end{aligned} \quad (20)$$

Based on the boundary conditions of k_ν chosen, the relationship between k_ν and K_ν is rewritten by:

$$\begin{aligned} k_p = 1000 + 2500K_p; \quad k_i = 1 + 199K_i; \\ \text{and} \ \ k_d = 0.1 + 19.9K_d. \end{aligned} \quad (21)$$

By replacing Eq. (21) to (19), the active damping force "u" of the PID controller is rewritten as:

$$\begin{aligned} u = (1000 + 2500K_p)\, e + (1 + 199K_i) \int_0^t e\, dt + \\ (0.1 + 19.9K_d)\, \dot{e}. \end{aligned} \quad (22)$$

To determine the variables of K_ν via the fuzzy controller, the fuzzy controller is established including the fuzzification interface, fuzzy inference system, and defuzzification interface. "First, the crisp values in fuzzification are transformed into linguistic variables, Fuzzy inference system is then used by control rules in accordance with inference rules, and finally, the linguistic variables are transformed back to crisp values via defuzzification for use by the physical plant".[30] Thus, the design of the fuzzy controller is performed in three steps as follows:

Table 2. The LV and its numerical value.

Input value			Output value	
LV	ec	e	LV	K_ν
PB	0.22	0.012	B	1.0
PS	0.11	0.006	MB	0.8
Z	0	0	M	0.6
NS	–0.11	–0.006	MS	0.4
NB	–0.22	–0.012	S	0.2

Table 3. The fuzzy rule in the Fuzzy-PID controller.

K_p		ec				
		PB	PS	Z	NS	NB
e	PB	MB	B	M	MS	S
	PS	MB	M	S	M	MS
	Z	M	MS	S	MS	B
	NS	MS	M	S	M	MB
	NB	S	MS	M	MB	M
K_i		ec				
		PB	PS	Z	NS	NB
e	PB	S	S	MB	M	S
	PS	S	MB	M	MS	MB
	Z	MS	M	S	MB	M
	NS	M	S	MS	B	S
	NB	M	MS	MS	S	S
K_d		ec				
		PB	PS	Z	NS	NB
e	PB	M	MS	MS	S	B
	PS	S	MS	S	M	MB
	Z	S	S	S	M	B
	NS	B	MS	B	S	M
	NB	MS	MB	M	MS	S

Step 1: Set the language variable (LV) of input and output values. The LV of two input values (e and ec) is established by the Negative-Big (NB), Negative-Small (NS), Zero (Z), Positive-Small (PS), and Positive-Big (PB). Besides, the LV of three output values (K_ν) is also established by the Small (S), Medium-Small (MS), Medium (M), Medium-Big (MB), and Big (B). The values of e, ec, and K_ν are defined in Table 2.

Step 2: Set the membership function. The shape of the membership functions of the input/output variables in the fuzzy controller is established by the Triangular function.

Step 3: Set the control rules of the fuzzy controller. The efficiency of the fuzzy controller is strongly affected by its control rules.[31] Therefore, to enhance the control efficiency, the control rules in the Fuzzy-PID controller optimized by the genetic algorithm in the paper of Nguyen et al.,[5] as listed in Table 3, are applied to control the K_ν. Based on the optimal control rules in Table 3, the control rules of the input/output variables in the fuzzy controller are built by:
(1) If e is NB and ec is NB then K_p is M, K_i is S, K_d is S,
(2) If e is NB and ec is NS then K_p is MB, K_i is S, K_d is MS,
...
(25) If e is PB and ec is PB then K_p is MB, K_i is S, K_d is M.

The fuzzy inference system used by the minimum function and centroid method in the fuzzy controller is then applied to calculate the output parameters of K_ν based on the input parameters of e, ec, and the control rules of the fuzzy controller.

Table 4. The soil compactor's dynamic parameters.

Parameters	Values	Parameters	Values
m_s / kg	85	$k_{w1,2}$ / MN m^{-1}	0.5
m_c / kg	891	l_1 / m	0.383
m_{fb} / kg	2822	l_2 / m	0.1
m_{rb} / kg	4464	l_3 / m	0.524
m_d / kg	4378	l_4 / m	0.136
$c_{c1,2}$ / Ns m^{-1}	218	l_5 / m	0.6
$c_{c3,4}$ / Ns m^{-1}	29	l_6 / m	0.76
$c_{h1,2}$ / kNs^2 m^{-2}	20	l_7 / m	0.9
$c_{h3,4}$ / kNs^2 m^{-2}	4.5	l_8 / m	1.5
$c_{d1,2}$ / kNs m^{-1}	2.9	b_1 / m	0.55
$c_{w1,2}$ / kNs m^{-1}	4.0	b_2 / m	0.7
$k_{c1,2}$ / MN m^{-1}	0.91	b_3 / m	0.68
$k_{c3,4}$ / MN m^{-1}	0.12	b_4 / m	0.945
$k_{d1,2}$ / MN m^{-1}	3.9	b_5 / m	0.945

4. RESULTS AND ANALYSIS

4.1. Evaluation Index of the Ride Quality

The indices of ride quality, suspension deformation, and road friendliness were directly applied to assess the efficiency of the vibration isolation systems.[3,4,9] With the driver's seat isolation, the ride quality calculated through the weighted root-mean-square of the seat acceleration (a_{ws}) in the time region was applied.[4,11,12] In addition, according to the standard of ISO 2631-1,[7] the power spectral density (PSD) of the acceleration response was also used to evaluate the influence of vibration on the endurance limit of the human body in the low frequency region below 10 Hz. Especially, at a low frequency range of $0.5-4.0$ Hz seriously affected the driver's health and safety. The a_{ws} of the driver's seat was expressed by:[7,11]

$$a_{ws} = \sqrt{\frac{1}{T}\int_0^T \ddot{z}_s^2(t)\,dt}; \tag{23}$$

where $\ddot{z}_s(t)$ is the seat's acceleration response depending on the simulation time T.

Therefore, to assess the soil compactor's ride quality with the seat suspension equipped with the SAC and NSS, the reduction of the a_{ws} and maximum PSD value of the driver's seat is selected as the objective function.

4.2. The Seat's Response under Three Different Vehicle Models

Under the condition of the soil compactor moving and compacting on the elastoplastic soil ground, the vehicle's ride comfort was greatly affected.[1–4] Thus, based on the lumped parameters of the soil compactor in Table 4,[5] the parameters of the elastoplastic soil ground at the rigid drum and wheel in Table 5,[1,21] and the poor surface roughness of the deformable soil ground in Fig. 4; the 1-D, 2-D, and 3-D dynamic models of the soil compactor in Fig. 1a, 1b, and 1c with the seat passive suspension in Fig. 8a are simulated when the vehicle is compacting on the elastoplastic soil ground at an excitation frequency 35 Hz of the drum to evaluate the influence of three dynamic models on the seat's vibration response. The simulation results of the seat's vibration response are plotted in Fig. 8b, 8c, and 8d.

Figure 8b is the acceleration response of the driver's seat under three different vehicle models. The result shows that the

Table 5. The parameters of the elastoplastic soil ground.

Parameters	Values	Parameters	Values
Elastoplastic soil's characteristic under the rigid drum			
ε	0.34	k_{es} / MN m^{-1}	12.5
c_{es} / kNs m^{-1}	70	k_{ps} / MN m^{-1}	6.44
Deformable soil's characteristic under the wheel			
θ / °	28	k / kN m^{-n-1}	6.94
c / kPa	1.3	k_θ / MN m^{-n-2}	0.506

Table 6. The maximum PSD acceleration of the driver's seat.

Vehicle models	1-D	2-D	3-D
f / Hz	2.299	1.899	1.899
PSD / m^2 s^{-3}	1.157	0.598	0.480

seat's acceleration response with the three different models is the same. However, the seat's acceleration response with the 1-D model is higher than that of both 2-D and 3-D models, whereas the seat's acceleration response with the 2-D model slightly deviates in comparison with the 3-D model. The calculation results in Fig. 8c indicate that the a_{ws} of the 1-D model is higher than that of the 2-D and 3-D models by 29.1% and 35.9%, while the a_{ws} with the 2-D model is higher than that of the 3-D model by 9.6%. The a_{ws} of the 1-D model is higher than that of 2-D and 3-D models may be due to the influence of the vibration excitations of elastoplastic soil ground, poor surface roughness, and vibratory drum acts directly on the driver's seat in the vertical direction via the vibration isolation systems of the soil compactor, as shown in Fig. 1a. Conversely, the a_{ws} of the 3-D model is slightly deviated compared to the 2-D model under the same excitations of the elastoplastic soil ground and vibratory drum may be due to the influence of the horizontal deflection b_1 of the driver's seat in the 3-D model relative to the vehicle's center of gravity while the value $b_1 = 0$ in the 2-D model, as shown in Fig. 1b and 1c.

The PSD acceleration of the driver's seat in Fig. 8d also indicates that the PSD acceleration with the 1-D model is higher than that of the 2-D and 3-D models, whereas the PSD accelerations of the 2-D and 3-D models are similar. Based on the maximum PSD acceleration of the driver's seat listed in Table 6, the maximum PSD value with the 1-D model is higher than that of the 2-D and 3-D models by 48.3% and 58.5%, while the maximum PSD value between 2-D and 3-D models is slightly deviated by 19.7%. From the analysis result of the seat's acceleration and PSD acceleration in both time and frequency regions, we can see that the dynamic model of the soil compactor greatly affects the calculation results, especially between 1-D and 3-D models. If the vehicle dynamic model is more similar to the actual vehicle then the simulation result is more accurate. However, in the existing studies on seat suspension using the SAC and NSS, the dynamic model of the vehicle was mainly established by the 1-D model.[9–15] This can significantly affect the efficiency of the SAC and NSS. Thus, the 3-D vehicle dynamic model should be used to evaluate the efficiency of the SAC and NSS. To further elucidate the accuracy of the mathematical model of the 3-D dynamic model, the experimental study of the soil compactor is made in Section 4.3.

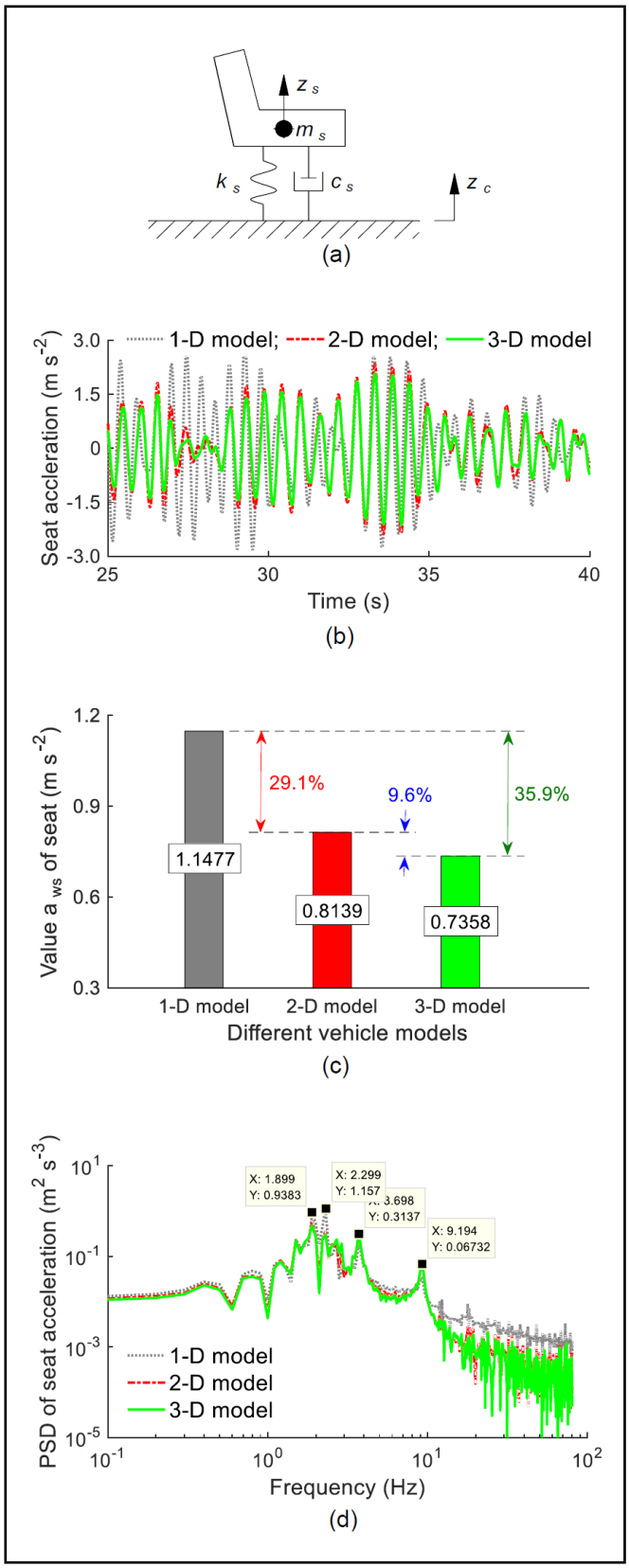

Figure 8. The seat passive suspension without the SAC and NSS (a), the seat acceleration in the time domain (b), calculation value a_{ws} of seat (c), and PSD of seat acceleration in the frequency domain (d).

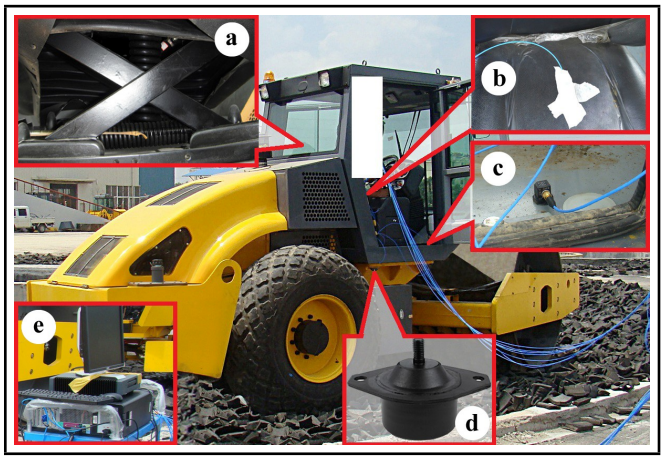

Figure 9. The experiment of the soil compactor using the seat suspension embedded by the NSS and cab hydraulic mounts. Where (a) is the NSS, (b) is the acceleration sensor on the seat, (c) is the acceleration sensor on the cab floor, (d) is the hydraulic mounts, and (e) is the display of the measured results.

4.3. Experiment with the Soil Compactor

To verify the accuracy of the 3-D vehicle dynamic model, an actual soil compactor with the cab hydraulic mounts and seat suspension embedded by the NSS has been tested. The test condition is carried out under the same simulation conditions of the vehicle in Section 4.2 and the test setup is depicted in Fig. 9. To measure the seat's acceleration response and PSD acceleration, a 3-D acceleration sensor of ICP®is installed on the driver's seat to measure the seat's acceleration response. Then, a dynamic test and analysis system of the Belgium LMS is used to analyze the signal and display the results. Based on the test results, the seat's acceleration response and PSD acceleration have been plotted in Fig. 10a and 10b, respectively.

In observing Fig. 10a, the seat's acceleration response of the simulation is similar to that of the experiment. Based on the seat's acceleration response in Fig. 10a, the calculation result of the a_{ws} of the measurement and simulation is obtained by $0.2385\ \mathrm{m\,s^{-2}}$ and $0.2157\ \mathrm{m\,s^{-2}}$; and the a_{ws} of the simulation is only deviated by 9.6% compared to the measurement.

Figure 10b also shows that the resonance peaks of the seat's PSD acceleration of the simulation are also similar to the measurement in both the trends and responses. However, the a_{ws} and PSD acceleration of the driver's seat between the simulation and measurement have a small error. This is due to the influence of some assumptions of the 3-D vehicle dynamic model in Section 2 and the NSS's model in Section 3.1; and the influence of some deviations in the installation of the measuring equipment and vehicle dynamic parameters. However, these errors are quite small and could be accepted. Therefore, the experiment's result proves that the simulation result with the 3-D model is more accurate than the 1-D model of the soil compactor.

Based on the numerical simulation and experimental results of the 3-D vehicle dynamic model in Sections 4.2 and 4.3, we can see that the obtained efficiency of the SAC or NSS of the seat suspension using the 3-D model is smaller than that of the 1-D and 2-D models. However, the 3-D model is like the actual model of the soil compactor. Thus, the use of the 3-D vehicle dynamic model can accurately evaluate the actual

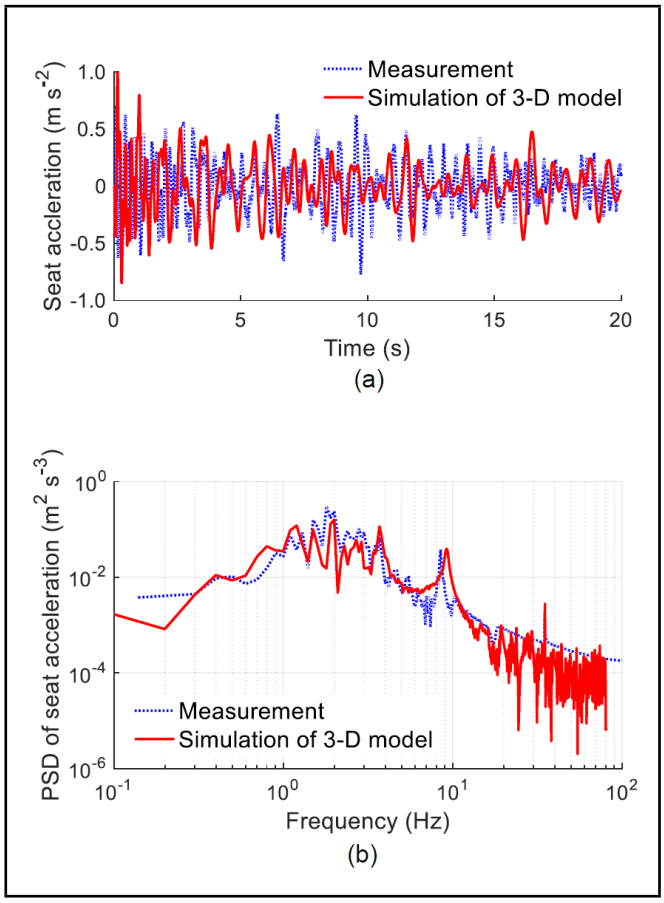

Figure 10. The result of the simulation and measurement of the seat acceleration in the time domain (a) and PSD of seat acceleration in the frequency domain (b).

Table 7. The NSS's parameters.

Parameters	Values	Parameters	Values
a / m	0.286	α	0.63
k_s / kN m^{-1}	5.8	β_1	0.73
c_s / Ns m^{-1}	120	β_2	1.17

efficiency of the SAC or NSS applied on the seat suspension of the soil compactor. This means that the driver's ride comfort of the soil compactor with the seat suspension equipped with the SAC or NSS is also accurately evaluated according to the standard of ISO 2631-1.[7] This is also the advantage of the 3D model compared to others. Therefore, the 3-D dynamic model of the soil compactor is applied to evaluate the actual efficiency of the seat suspension equipped with the SAC and NSS (SAC+NSS) on improving the ride comfort of the soil compactor in Section 4.4.

4.4. Efficiency of Seat Suspension Equipped with SAC and NSS

Based on the control model of the Fuzzy-PID controller for the seat suspension in Section 3.2 and the parameters of the NSS in Table 7,[11] the 3-D dynamic model of the soil compactor is used to evaluate the efficiency of the SAC+NSS under the same simulation condition in Section 4.2. The simulation results of the seat's vibration response are plotted in Fig. 11.

The simulation result in Fig. 11a shows that the seat's acceleration response with the SAC (control suspension of the

Table 8. The maximum PSD acceleration of the driver's seat.

Seat's isolation	SPS	SAC	NSS	SAC+NSS
PSD / $m^2\,s^{-3}$	0.621	0.253	0.159	0.077

seat without the NSS) is significantly reduced in comparison with the seat passive suspension (SPS). This is due to the active force u in Eq. (22) controlled by the Fuzzy-PID controller impacting the seat suspension to reduce the seat's vibration. With the NSS (passive suspension of the seat embedded by the NSS), the seat's acceleration response is greatly reduced compared to both SAC and passive suspension without the NSS. This is due to the impaction of the total restoring force F_R of the vertical and horizontal springs of the NSS in Eq. (15). The NSS's efficiency in improving the seat's ride comfort is better than without the NSS, which has been demonstrated in the existing researches.[13–16] However, this study also shows that with the seat suspension embedded by the NSS, the seat's acceleration response is lower than that of the SAC. This means that the efficiency of the NSS in improving the seat's ride comfort is better than the SAC. This issue has not been researched in the existing studies.

With the SAC+NSS, the result indicates that the seat's acceleration response is smaller than that of the NSS. This can be due to the impaction of both the active force u and the total restoring force F_R. Besides, the results of the a_{ws} are also calculated and compared in Fig. 11b. In observing Fig. 11b, we can see that the a_{ws} with the SAC, NSS, and SAC+NSS is greatly reduced by 24.1%, 70.7%, and 80.1% in comparison with the passive suspension of the seat, respectively. This study result shows that the efficiency of the SAC and NSS is similar to the study results in the publications of Kumar et al.,[10] Hosseini and Marzbanrad,[11] Saini,[14] and Akintoye.[15] Especially with the seat suspension equipped with both SAC and NSS, its isolation efficiency is also better than that of each SAC and NSS. Therefore, the soil compactor's ride comfort with the SAC+NSS is better improved compared to both the SAC and NSS.

In addition, the seat's acceleration response in the frequency region is also used to evaluate the efficiency of the SAC+NSS. The seat's PSD acceleration in Fig. 11c shows that the seat's PSD acceleration with the SAC, NSS, and SAC+NSS is significantly reduced in comparison with the seat's passive suspension, especially with the SAC+NSS. This is also due to the impaction of both the active force u and the total restoring force F_R. In particular, at low frequencies below 4.0 Hz which greatly affects the driver's health and safety,[7] the calculation results in Table 8 indicate that the maximum PSD acceleration of the driver's seat with the SAC, NSS, and SAC+NSS is greatly reduced by 59.3%, 74.4%, and 87.6% compared to the seat's passive suspension, respectively, especially with the SAC+NSS. Based on the above analysis result, it can be concluded that the seat suspension equipped with both SAC and NSS greatly improves the vehicle's ride comfort in both the time and frequency regions. However, the above results only simulate under one working condition of the vibratory, to fully evaluate the efficiency and stability of both SAC and NSS, the change of the driver's seat mass and vehicle's moving velocity is also simulated in Section 4.5.

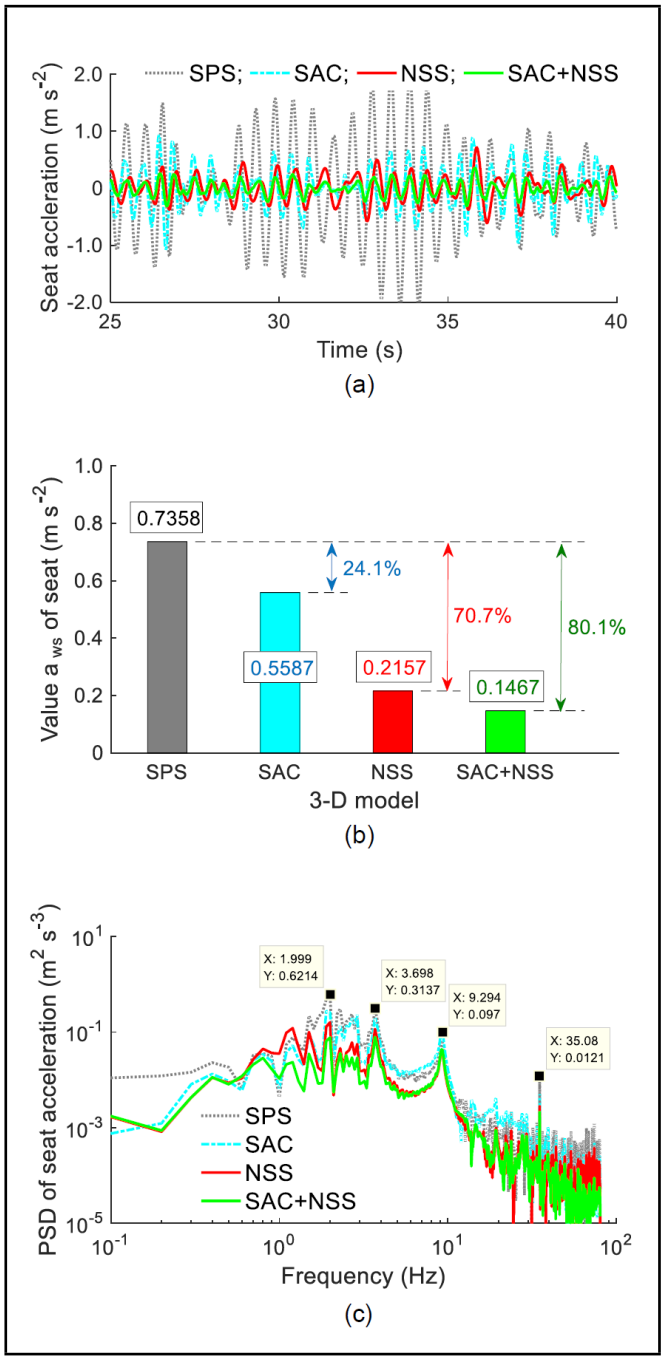

Figure 11. The seat acceleration in the time domain (a), calculation value a_{ws} of seat (b), and PSD of seat acceleration in the frequency domain (c) using the 3-D vehicle model.

4.5. Efficiency under Different Vehicle Conditions

Under the same simulation condition in Section 4.2, the driver's seat mass and vehicle's moving velocity are changed to evaluate the efficiency and stability of the SAC+NSS. With the driver's mass changed by $m_s = [60, 65, \ldots, 110]$ kg, the simulation result is plotted in Fig. 12a. The simulation result shows that the a_{ws} is reduced with the increase of the driver's seat mass and vice versa, especially with the seat passive suspension. Therefore, the driver's seat mass significantly affects the driver's ride comfort. However, with the SAC+NSS, the result shows that the a_{ws} not only is lower than that of the SAC and NSS but also more stable when the driver's seat mass is

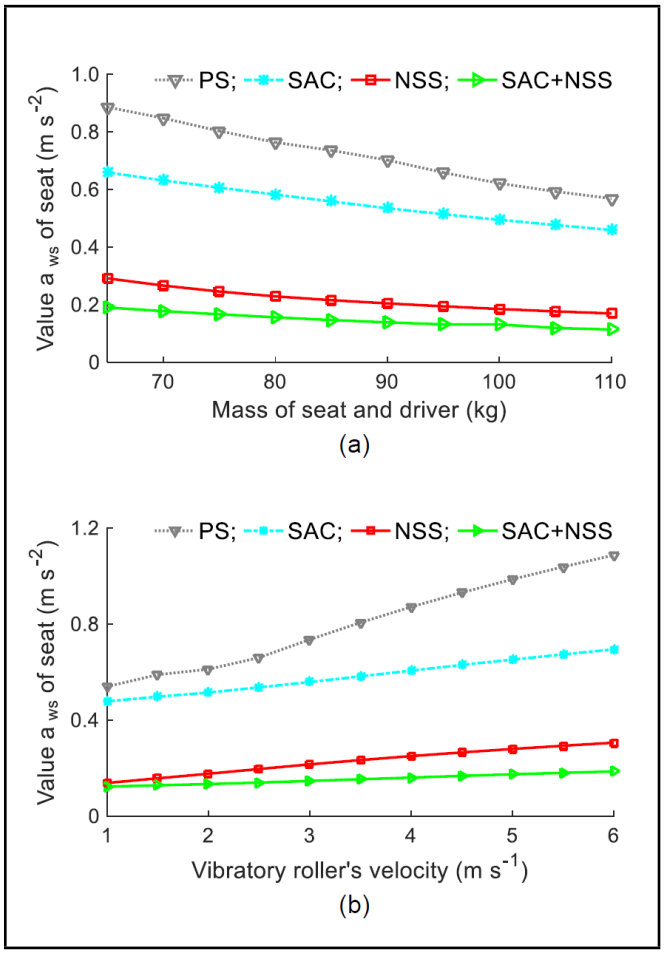

Figure 12. Seat's acceleration response under different driver's mass (a) and different soil compactor's moving velocities (b).

changed.

With the change of the soil compactor's moving velocity $v_0 = [1.0, 1.5, \ldots, 6]$ km h^{-1}, the simulation result of the a_{ws} with different isolations of the driver's seat is plotted in Fig. 12b. The result shows that the a_{ws} is strongly increased when the moving velocity is increased. This means that the driver's ride comfort is reduced with the increase of the vehicle's moving velocity. With the SAC+NSS, the a_{ws} is strongly reduced in comparison with both the SAC and NSS under various moving velocities of the soil compactor. Thus, it can conclude that the seat suspension equipped with the SAC and NSS can remarkably improve the driver's ride comfort under the various conditions of the soil compactor.

5. CONCLUSIONS

The seat's vibration response with the seat passive suspension using 1-D, 2-D, and 3-D dynamic models of the soil compactor was similar. However, the a_{ws} and maximum PSD acceleration of the driver's seat with the 1-D model were higher than that of the 3-D model by 35.9% and 58.5%, while the seat's acceleration response and PSD acceleration of the simulation using the 3-D dynamic model were similar to the experiment. Therefore, the choice of vehicle dynamic model greatly affects the investigation result.

With the SAC+NSS, the a_{ws} and maximum PSD acceleration of the driver's seat were greatly reduced by 80.1% and 87.6% in comparison with the seat passive suspension. Additionally, these values were also lower than that of both the SAC and NSS under various simulation conditions. Therefore, the seat suspension equipped with the SAC and NSS should be applied to further enhance the soil compactor's ride comfort.

This study also provides an important reference for the application of the NSS and the semi-active control of the seat suspension of other vehicles to improve ride quality.

ACKNOWLEDGEMENTS

This research is supported by the Science and Technology Support Program of Handan (No. 1721212044) and Science and Technology Research Project of the Education Department of Hebei Province, (No. QN2019326).

REFERENCES

[1] Adam, D. and Kopf, F. Theoretical analysis of dynamically loaded soils, *European Workshop Compaction of Soils and Granular Materials*, Paris, 207–220, (2000).

[2] Kordestani, A., Rakheja, S., Marcotte, P., Pazooki, A., and Juras, D. Analysis of ride vibration environment of soil compactors, *SAE International Journal Commercial Vehicle*, **3**, 259–272, (2010). https://doi.org/10.4271/2010-01-2022

[3] Le, V. *Vibration study and control for cab of vibratory roller*, Southeast University, Nanjing, China, (2013).

[4] Nguyen, V., Zhang, J., Le, V., and Jiao, R. Vibration analysis and modeling of an off–road soil compactor equipped with three different cab's isolation mounts, *Shock and Vibration*, **2018**, 1–17, (2018). https://doi.org/10.1155/2018/8527574

[5] Nguyen, V., Jian, R., and Yang, Z. Low–frequency performance of semi-active cab's hydraulic mounts of an off-road soil compactor, *Shock and Vibration*, **2019**, 1–15, (2019). https://doi.org/10.1155/2019/8725382

[6] Hua, W., Liem, N., and Hua, X. Experimental investigation and vibration control of semi-active hydraulic–pneumatic mounts for soil compactor cab, *SAE International Journal of Vehicle Dynamics, Stability, and NVH*, **5**, 1–15, (2021). https://doi.org/10.4271/10-05-04-0028

[7] ISO 2631-1 Mechanical vibration and shock—Evaluation of human exposure to wholebody vibration—Part 1: General requirements, International Organization for Standardization, Geneve, Switzerland, (1997).

[8] Yuan, H., Nguyen, V., Jiao, R., and Le, V. Analyzing the accuracy of the air suspension system models based on two different calculation methods, *SAE International Journal of Vehicle Dynamics, Stability, and NVH*, **5**, 459–473, (2021). https://doi.org/10.4271/10-05-04-0031

[9] Hostens, I., Deprez, K., and Ramon, H. An improved design of air suspension for seats of mobile agricultural machines,

Journal of Sound and Vibration, **276**, 141–156, (2004). https://doi.org/10.1016/j.jsv.2003.07.018

[10] Kumar, S., Medhavi, A., and Kumar, R. Active and passive suspension system performance under random road profile excitations, *International Journal of Acoustics and Vibration*, **25**, 532–541, (2020). https://doi.org/10.20855/ijav.2020.25.41702

[11] Hosseini, S. and Marzbanrad, J. Robust H-infinity controller in a MRF engine mount for improving the vehicle ride comfort, *International Journal of Acoustics and Vibration*, **25**, 219–225, (2020). https://doi.org/10.20855/ijav.2020.25.21592

[12] Mohd, H., Wong, J., and Ahmad, Z. Numerical approach on hybrid PID-AFC controller using different intelligent tuning methods to reduce the vibration of the suspended handle, *International Journal of Acoustics and Vibration*, **26**, 28–40, (2021). https://doi.org/10.20855/ijav.2020.25.11713

[13] Zha, J., Nguyen, V., Su, B., Jiao, R., and Ni, D. Performance of the seat suspension system using negative stiffness structure on improving the driver's ride comfort, *SAE International Journal of Vehicle Dynamics, Stability, and NVH*, **16**, 135–146, (2022). https://doi.org/10.4271/10-06-02-0009

[14] Saini, M. Modelling and simulation of vehicle suspension system with variable stiffness using quasi-zero stiffness mechanism, *SAE International Journal of Vehicle Dynamics, Stability, and NVH*, **4**, 37–47, (2020). https://doi.org/10.4271/10-04-01-0003

[15] Akintoye, O. Experiment study on nonlinear oscillator containing magnetic spring with negative stiffness, *International Journal of Non-Linear Mechanic*, **120**, 103396, (2020). https://doi.org/10.1016/j.ijnonlinmec.2019.103396

[16] Li, S., Nguyen, V., Jiao, R., Ni, D., and Zhou, H. Isolation efficiency of vehicle seat suspension with three quasi-zero stiffness models, *International Journal of Acoustics and Vibration*, **27**, 1–13, (2022). https://doi.org/10.20855/ijav.2022.27.31858

[17] Zhang, Y., Wei, G., Wen, H., Jin, D., and Hu, H. Design and analysis of a vibration isolation system with cam–roller–spring–rod mechanism, *Journal of Vibration and Control*, (2021). https://doi.org/10.1177/10775463211000516

[18] Zha, J., Nguyen, V., Ni, D., and Su, B. Optimizing the geometrical dimensions of the seat suspension equipped with a negative stiffness structure based on a genetic algorithm, *SAE International Journal of Vehicle Dynamics, Stability, and NVH*, **16**, 11–20, (2022). https://doi.org/10.4271/10-06-02-0010

[19] Le, T. and Ahn, K. A vibration isolation system in low frequency excitation region using negative stiffness structure for vehicle seat, *Journal of Sound and Vibration*, **330**, 6311–6335, (2011). https://doi.org/10.1016/j.jsv.2011.07.039

[20] Shi, X. and Zhu, S., Magnetic negative stiffness dampers, *Smart Materials and Structure*, **24**, 072002, (2015). https://doi.org/10.1088/0964-1726/24/7/072002

[21] Shi, X. and Zhu, S., Simulation and optimization of magnetic negative stiffness dampers, *Sensors and Actuators A: Physical*, **259**, 14–33, (2017). https://doi.org/10.1016/j.sna.2017.03.026

[22] Dong, G., Zhang, X., Xie, S., Yan, B., and Luo, Y. Simulated and experimental studies on a high-static-low-dynamic stiffness isolator using magnetic negative stiffness spring, *Mechanical Systems and Signal Processing*, **86**, 188-–203, (2017). https://doi.org/10.1016/j.ymssp.2016.09.040

[23] Wang, M., Hu, Y., Sun, Y., Ding, J., Pu, H., Yuan, S., Zhao, J., Peng, Y., Xie, S., and Luo, J. An adjustable low-frequency vibration isolation stewart platform based on electromagnetic negative stiffness, *International Journal of Mechanical Sciences*, **181**, 105714, (2020). https://doi.org/10.1016/j.ijmecsci.2020.105714

[24] Yan, B., Yu, N., and Wu, C. A state-of-the-art review on low-frequency nonlinear vibration isolation with electromagnetic mechanisms, *Applied Mathematics and Mechanics*, **43**, 1045–1062, (2022). https://doi.org/10.1007/s10483-022-2868-5

[25] Bekker, M. *Introduction to terrain-vehicle systems*, University of Michigan Press, Ann Arbor, (1969).

[26] Zhang, X. *Modelling, simulation and optimization of ride comfort for off road articulated dump trucks*, Southeast University, Nanjing, China, (2010).

[27] Wong, J. *Theory of ground vehicles*, John Wiley & Sons Inc, New York, (2001).

[28] ISO/TC108/SC2/WG4 N57, Reporting vehicle road surface irregularities, (1982).

[29] Mitschke, M. *Dynamik der kraftfahrzeuge*, Springer–Verlag, Berlin, (1972). https://doi.org/10.1007/978-3-662-11585.5

[30] Nguyen, V., Wu, Z., Zhang, B., and Run Z. J. Vibration analysis and control of a vibration screed system for asphalt pavers, *International Journal of Acoustics and Vibration*, **25**, 363–372, (2020). https://doi.org/10.20855/ijav.2020.25.31649

[31] Mamdani, E. and Assilian, S., An experiment in linguistic synthesis with a fuzzy logic controller, *International Journal Man-Machine Studies*, **7**, 1—13, (1975). https://doi.org/10.1016/S0020-7373(75)80002-2